

Theoretical and experimental analysis on the interaction properties between tracks and sediments considering sand content for unmanned underwater tracked bulldozer

Yong LI^{1*}, Dingchang HE¹, and Qiaorui SI²

¹Automotive Engineering Research Institute, Jiangsu University, Zhenjiang, 212013, P. R. China

²Research Center of Fluid Machinery Engineering and Technology, Jiangsu University, Zhenjiang, 212013, P. R. China

Abstract. The unmanned underwater tracked bulldozer (UUTB) is an indispensable equipment for dredging and cleaning obstacles on the river bed in the flood season. The investigation on the interaction properties between the UUTB tracks and sediments provides foundation for the evaluation of operation performance when it works on the inland river bed. Based on the current worldwide research, the sediments mixed by sand, bentonite and water with sand content 0%, 10% and 20% were configured in this study to replace the real sediments on the inland river bed in China. The current pressure-sinkage model and shear stress-shear displacement model were discussed. Three different tracks were tested for the pressure-sinkage and the shear stress-shear displacement on the platform. The relationship between pressure and sinkage under sand content 0%, 10% and 20% are revealed based on the experimental results. The modulus of cohesive deformation and friction deformation of the sediments under said sand content are presented. The curves of shear stress and shear displacement are also obtained, which demonstrates the properties between the tracks and configured sediments under sand content 0%, 10% and 20%. The relationship between the tractive force and slip ratio with three different tracks under said sand content is also presented based on the quantitative analysis, which provides reference for the dynamics control and performance evaluation of UUTB on the inland river bed.

Key words: unmanned underwater tracked bulldozer; underwater robot; river bed sediment; shear stress; pressure-sinkage.

1. Introduction

With the accelerating process of urbanization and the impact of global climate changes, cities in China, especially coastal cities, are facing the risk of stagnant water. In recent years, according to the survey, there have been frequent incidents of urban rainwater in China, and the frequency of urban waterlogging has shown an increasing trend. Inevitably, the urban waterlogging will cause some problems such as siltation of river rocks and sediments, narrowing and shallowing of rivers, etc., which limits the drainage function of inland rivers in the inland flood season. Besides, the urban waterlogging not only threatens the safety of public life and property, but also has a serious impact on the national or regional economy [1, 2]. Dredging in rivers and dredging work is an important measure to quickly restore the drainage function of urban inland rivers. However, traditional mechanical dredging equipment (such as dredgers) has the disadvantages of large size, single function, high operating cost, poor flexibility and low level intelligence, which cannot meet the requirements of dredging and dredging operations in urban inland rivers [3]. With this background, it is necessary to develop a new unmanned underwater tracked bulldozer (UUTB) with the functions of dredging, pushing and towing.

Compared with tradition dredgers, UUTB is an effective equipment to complete the dredging work of the inland rivers in the flood season. The dynamic coupling properties analysis is the key technique for UUTB dynamics due to its harsh and unexpected working environment. The mechanical properties between underwater tracked bulldozer tracks and the river sediments provide foundations for the analysis of dynamic coupling properties. Komatsu Company in Japan first developed the D155W underwater bulldozer in early 1968. The bulldozer controlled wireless or by wire operates at a 7-meter water depth [4]. In January 2013, the underwater bulldozer played an essential role in the reconstruction work after the earthquake and tsunami in Japan. In addition, Komatsu, Hitachi and other companies in Japan have also developed underwater bulldozers operating at 15 to 60 meters depth. However, the dynamics analysis of tracked underwater bulldozer is still in a confidential stage due to the rigorous technical protection in Japan, and the corresponding papers and patents are rare. There is still no research on UUTB in China.

As typical underwater equipment, the study on mechanical properties of the interaction between the undersea mining vehicle track and the seabed sediment provides a reference for that of the underwater bulldozer track and inland river sediment [5, 6]. A lot of research has been done on the mechanical properties of undersea miner tracks and seabed sediments. Hong established the transient dynamics model of a tracked undersea miner operating on a soft bottom of the seabed and simplified the vehicle body into a six-degree-of-freedom

*e-mail: liyongthinkpad@outlook.com

Manuscript submitted 2020-04-23, revised 2020-10-21, initially accepted for publication 2020-11-10, published in February 2021

model. The curves of shearing force and displacement, sinkage and pressure, dynamic subsidence and shearing force are presented to describe the mechanical properties of soft sediments on the seabed [7]. Yoon investigated the studied tractive performance of tracked vehicles walking on the extremely soft soil and analyzed various parameters including track speed, track grouser shape, track grousers span, vehicle weight and gravity position, which effect tractive performance of the vehicle [8]. Herzog and Schulte focused on the interaction properties between the mining vehicle track and the sediments on the seabed, and also studied its impact on the dynamics performance while the vehicle was operating on the seabed [9]. Grebe and Schulte proposed a method based on the actual measurement data of the tracked mining vehicle to obtain the soil mechanical parameters of the seabed and described the relationship between the tractive force of the mining vehicle and the seabed soil parameters [10]. Schulte and Schwarz analyzed the operating performance of tracked mining vehicle based on laboratory-measured mechanical properties of seabed sediments. The simulated sediments configured in the laboratory are combined by bentonite and water. The relationship between shearing force and displacement can be measured [11]. In China, Song in the State Oceanic Administration has studied the types of ocean sediments, geotechnical properties and soil strength [12]. Chen studied the physical properties of sediments in China's mining areas and obtained the seafloor sediment properties test data [13]. Liu and Dai investigated the mechanical properties between the track and configured sediments mixed by bentonite and water [14–18]. Based on Bekker and Reece theory, Li studied the relationship between load and sinkage of two types of sediments on the seabed of deep sea [19]. Wang proposed soft-plastic shear force-displacement (SPS) model based on the existing shear displacement empirical model and verified the model on the test platform [20, 21]. Yang worked on the track structure optimization with different soil mechanical properties and verified that on the test bed in the laboratory [22].

The vehicle-terramechanics of UUTB operating on the river bed mainly depends on the sand or rock content in the sediments of the river, which have a close relationship with the river location, hydrological condition and geological condition. The difference of sand content in different inland rivers is great, even in the same city [23, 24]. The UUTB operating on the soft sediments of inland rivers is employed to dredging and push the barrier while waterlogging occurs [25–27]. The difference of sand content does have an effect on the mechanical properties between the UUTB track and sediments on the inland river bed, which leads to further influence on the operation performance while the UUTB is working in the inland river. However, there is currently no investigation about mechanical properties analysis between UUTB track and inland river sediments with different sand content.

The contribution of this paper is to reveal the mechanical properties between the underwater bulldozer track and the sediments with different sand content, tracks are employed to test the mechanical properties on the test platform. The curve of pressure-sinkage and shearing force-displacement, tractive

force and slip ratio are obtained, which provide reference for the operation and anti-slip control of the UUTB.

The paper is organized as follows. First, in Section 2, the river bed sediments with different sand content are discussed. In Section 3, the mechanics of track-terrain interaction are discussed, and the tractive force is analyzed. After that, the experimental verification is presented in detail in Section 4. The test results about pressure-sinkage, shear stress-shear displacement and tractive force performance are also presented and discussed. Section 5 is devoted to the conclusions of the work.

2. River bed sediment configuration

2.1. River bed sediment analysis. There are many soil types in China due to its great geographical diversity. The temperature and rain falls increase from the north part to the south part of China. Therefore, the soil belts change with the latitude of the earth, which, from north to south, presents black soil, podzolic soil, yellow brown soil, red soil, yellow soil and latosol soil. The dry basis moisture of the soil decreases from eastern to western China. The components and particle size of all the soil types are totally different in China, even in one province due to the regional difference [28–30]

The Yangtze river, Yellow river, Heilongjiang river, Songhua river, Huai river, Liaohe river, Haihe river and Pearl river are the major natural rivers in China. The Beijing-Hangzhou grand canal is the famous artificial river in China. The soil erosion phenomenon is greatly influenced by the natural process and human activity. The deposition of the soil while flowing in the river constitutes the sediments on the river bed. The river sediment has a complex component, including soil, sand, small rock and decayed leaves. Furthermore, with the quick process of China's urbanization, more and more urban rivers are constructed artificially. The content of sand in the sediment of an artificial river is much higher than that of the traditional natural river, like the Yangtze river. To clearly figure out the sand content of the river sediment, the in-situ measurement was done in Zhenjiang city, Jiangsu province of China. The sediments of 4 sample dots from 2 rivers are collected and analyzed. The sediment is presented from a liquid flow state to plastic flow state with the increasing depth. The dry basis moisture and pore decrease with the increasing depth, and the wet density increases with the increasing depth [31–33]

2.2. River bed sediment configuration. The underwater bulldozer mainly works from 10 cm to 18 cm depth of the sediments, which provides the tractive force for the bulldozer. Data in Table 1 can be used as the reference in the simulated sediment configuration for the experiment. The mixture of bentonite and water is often used to delegate deep-sea sediments and tested in the laboratory. To simulate the real inland river sediments with certain sand content, the mixture of bentonite, sand and water is configured and tested to reveal their mechanical properties. Bentonite is one kind of clay mineral with white or light yellow colour [34]. It is composed by silica and alumina. Its molecular diameter is $10^{-11} \sim 10^{-9}$ m. Benton-

Table 1
Physical properties of the sediment sample

River sediments number	Dry basis moisture content (%)	Sand content (%)	Wet Density (g/cm ³)	Porosity ratio	Internal fraction angle (°)	Shear strength (kPa)
1	109	2	1.36	5.9	5.1	8.1
2	120	13	1.29	6.6	5.6	6.5
3	113	23	1.25	7.3	6.2	5.6
4	116	19	1.17	6.2	6.9	5.1

Table 2
Physical properties of the configured sediments

Configured Sediments number	Solid content		Dry basis moisture content (%)	Wet Density (g/cm ³)	Porosity ratio	Internal fraction angle (°)	Shear strength (kPa)
	Bentonite (%)	Sand (%)					
1	100	0	115	1.28	5.2	4.9	7.5
2	90	10	115	1.23	5.7	5.1	6.1
3	80	20	115	1.16	5.9	5.2	4.9

ite has good water absorption, expansibility and cohesiveness. The mixture of bentonite, sand and water will become one kind of soft clay, which has the properties of plasticity, cohesion and thixotropy.

The main physical properties of the configured sediments in the lab must agree with that of the sediments on the inland river bed [35]. The cross-cutting equipment is employed to test the physical and mechanical properties of the configured sediments in different positions of the test bed [36, 37]. The wet density, porosity ratio, internal fraction angle and shear strength of the configured sediments are shown in Table 2. The sediment should be left at least 24 hours after each disturbance. The sediments can be used to achieve good testing results until its physical properties in Table 2 are close to these in Table 1.

3. Mechanics of track-terrain interaction

The track is one of the main components of the underwater tracked bulldozer. The tractive force, adhesion force and braking force are transmitted to the vehicle body through the interaction with the sediments on the inland river bed, which is the precondition for the effective operation of the UUTB. The interaction between the track and sediment can be decomposed into two forms when the UUTB is operating on the river bed: track sinkage and track shearing, which is difficult to be tested at the same time in one experiment. The sinkage and shearing testing can be carried out, respectively.

3.1. Track model. The UUTB is facing technical problems under soft sediment while it is operating on inland river bed.

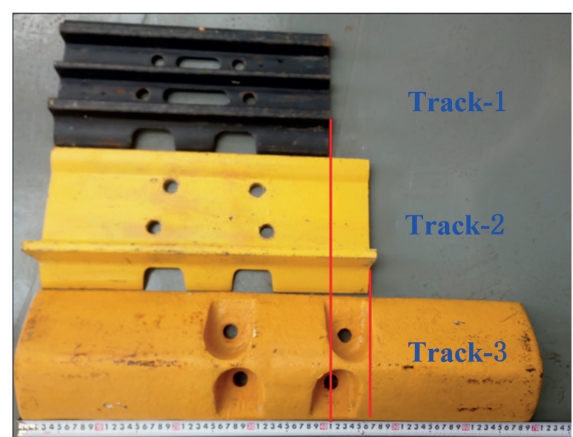
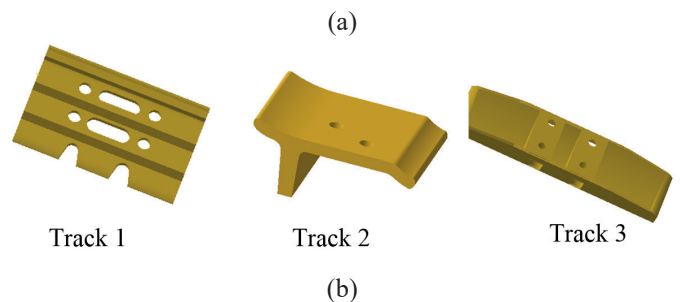


Fig. 1. Testing track shoe: a) 3D drawing, b) Real track

The operating performance is close to the track structure, which provides tractive force for the UUTB. Three different tracks shown in Fig. 1 are studied in this paper. The track parameters are shown in Table 3.

Table 3
 Bulldozer track parameters

Track	Width (cm)	Length (cm)	Height (cm)	Grounding connection area (cm ²)
1	40	20	4	0.08
2	46	18	6	0.0828
3	70	17	11	0.12

3.2. Shear stress-shear displacement properties. The shear stress and shear displacement will be caused by the interaction between the track and sediment when the UUTB is operating on the inland river bed, which provides the tractive force for the UUTB. The curve between the shearing force and displacement plays an essential role in characterizing the shearing strength of the sediment. Many researchers have investigated the shearing properties with different sediments. Wong, Schulte, Janosi-Hanamoto, Li and Wang proposed their own models, respectively.

Wong suggested using the empirical formula to calculate the influence of soil conditions on the tractive performance based on a large number of experimental tests [38–40]. The shear stress at any shear point in the sediment is expressed by Eq. (1):

$$\tau = \tau_{\max} K_r \left\{ 1 + \left[1 / (K_r (1 - 1/e)) - 1 \right] e^{(1-s/K_\omega)} \right\} (1 - e^{-s/K_\omega}), \quad (1)$$

where, τ_{\max} is the maximum shear stress, K_r is the residual shear stress divided by the maximum shear stress, s is the shear displacement, K_ω is the shear displacement at the maximum shear stress.

To evaluate the throughout ability of the sea bed sediment for the undersea mining vehicle, Schulte proposed the following empirical model through the saturated bentonite shearing test [41].

$$\tau = \tau_{\max} \left(e^{-b(s-K_\omega)} + K_r \right) \frac{1}{(f \cdot e^{-ds} + 1)}, \quad (2)$$

where, b is the attenuation index, f is the failure factor of the sediment, d is failure index of the sediment.

Janosi and Hanamoto model is widely used for land vehicles [42]. It is expressed as follows,

$$\tau = \tau_{\max} (1 - e^{-s/k}) (c + \sigma \cdot \tan \varphi) (1 - e^{-s/k}), \quad (3)$$

where, c is the land cohesion, φ is the land angle of internal friction, σ is the ground force, k is the shear modulus for land.

Li proposed the relationship between shear stress and shear displacement of configured sediments of deep sea through experiments [19].

$$\tau = \tau_{\max} \left(e^{-\frac{s}{k_1}} - e^{-\frac{s}{k_2}} \right) + \tau_{res} \left(1 - e^{-\frac{s}{k_2}} \right), \quad (4)$$

where, τ_{res} is residual shear stress, k_1 and k_2 are the coefficient, respectively.

Wang proposed a new empirical model shown as Eq. (5) for saturated soft-plastic soil to test the properties of seafloor soil [43, 44].

$$\tau = k_{pm} \cdot \left[- \left(e^{-s/K_\omega} - c_{pm} \right)^2 + (1 - c_{pm})^2 \right] \tau_{\max} + k_{pr} \cdot \left[\left(e^{-s/K_\omega} - c_{pr} \right)^2 - (1 - c_{pr})^2 \right] \tau_{res}, \quad (5)$$

where, c_{pm} is the correction factor caused by the soft-plastic deformation loss in hump zone, c_{pr} is the correction factor caused by the soft-plastic deformation loss in residual zone, k_{pm} is the adjustment coefficient of the hump part, k_{pr} is the adjustment coefficient of the residual part.

The above-mentioned shear stress-shear displacement models are widely used to investigate the physical properties between the track and soil for the operation performance of the tracked vehicle. The curve of shear stress and shear displacement is shown in Fig. 2. It can be seen from Fig. 2 that the shear stress increases sharply with the displacement of the track in the elastic deformation zone. After that, the elastic deformation of the sediment starts to fail while the shearing sediment mass gradually forms. In the sediment fracture zone, the shear stress drops sharply after the peak value of the shear stress. The shearing sediment starts to fracture, leading to the sliding of sediment mass. In the residual force zone, the shear stress slowly reduces to a stable residual shear stress. A lot of curves will be obtained when tracks with different length, width, height and grousers are tested with configured sediments under different sand contents.

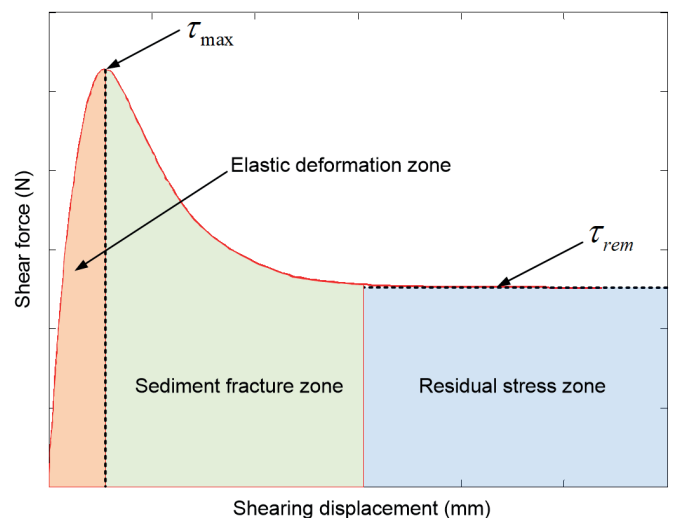


Fig. 2. Shear stress vs. shear displacement curve

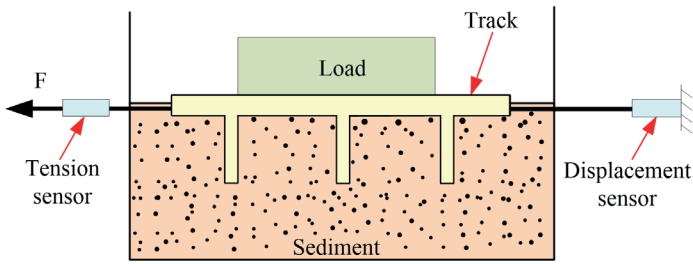


Fig. 3. Schematic diagram of shear stress-shear displacement

The schematic diagram of shear stress-shear displacement is shown in Fig. 3.

The track will move forward against the resistance of the sediment with a vertical downward load and forward force produced by a tractive motor. Three different tracks are tested in the paper. The shear stress is measured by a tension sensor. The displacement of the track is measured by a displacement sensor.

3.3. Pressure-sinkage properties. The sediment sinkage will occur to provide the supporting force when the bulldozer operates on the inland river bed due to its gravity. Many researchers have done a lot of research on the pressure-sinkage model.

Bekker model is widely used to describe the relationship between the pressure and sinkage, which is shown in Eq. (6) [45–47].

$$p = \left(\frac{k_c}{b} + k_\phi \right) z^n, \quad (6)$$

where, p is the vertical pressure, b is the track width. n is the sinkage coefficient, k_c and k_ϕ are the modulus of cohesive deformation and friction deformation of the sediment, respectively, z is the sinkage displacement.

Reece proposed a new empirical model shown in Eq. (7) between pressure and sinkage [48]

$$p = (ck'_c + b\gamma k'_\phi) \left(\frac{z}{b} \right)^n, \quad (7)$$

where, k'_c and k'_ϕ are the modulus of cohesive deformation and friction deformation of the sediment, respectively, γ_s is the sediment capacity.

The pressure-sinkage curve is shown in Fig. 4. The sediment will present elastic state, elastic-plastic state and plastic state, respectively, with the increase of the sinkage depth.

The driving resistance will be increased due to the river bed sinkage caused by the vertical load and pressure while the underwater bulldozer is operating on the bottom of the inland river. The properties of vertical load and deformation play an essential role to evaluate and predict the operating performance of the underwater bulldozer. The schematic diagram of pressure-sinkage is shown in Fig. 5. The above-mentioned three

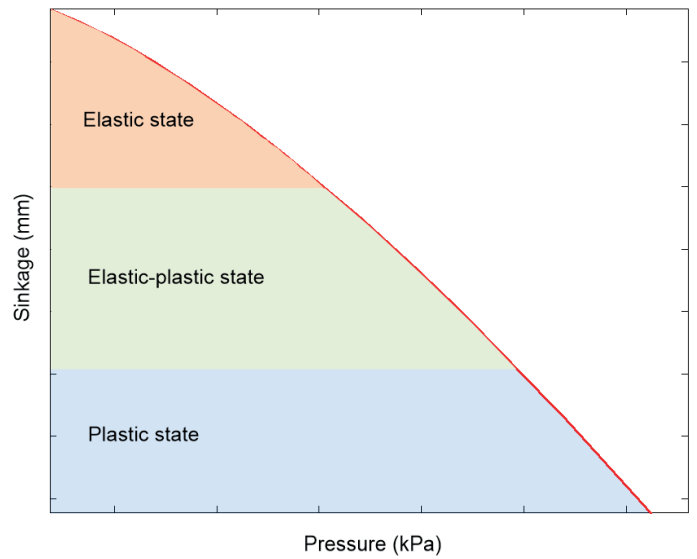


Fig. 4. Pressure vs. sinkage curve

tracks are tested to obtain the properties of pressure and sinkage. The track is vertically pressed into the configured sediment under the load motor. The pressure and track sinkage are measured and recorded by the pressure sensor and displacement sensor in the data acquisition system.

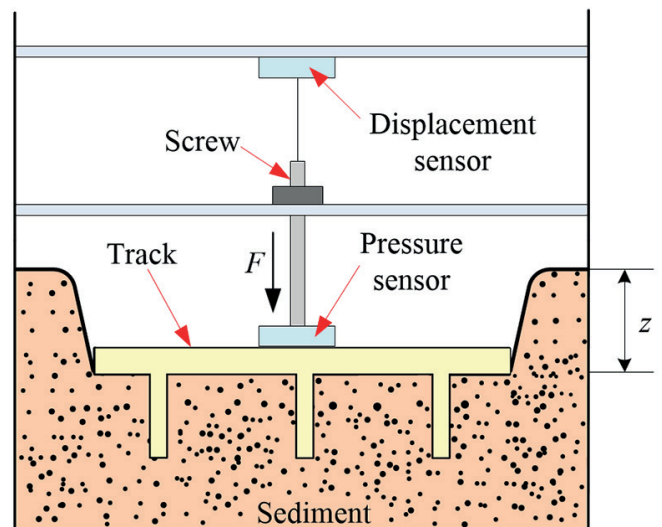


Fig. 5. Schematic diagram of pressure-sinkage

3.4. Tractive force analysis. The track sinks into the sediments under certain pressure. In this case, the interaction force that equals tractive force will be generated when the track is propelled inside the sediments. The schematic diagrams of different tracks are shown in Fig. 6a and Fig. 6b. l is the track length. h is the track height. P is the pressure implemented on the track. Z is the track sinkage. F_1 is the interactive force implemented by the sediments on the bottom of the track. F_2 is the interaction force implemented by the sediments on the track

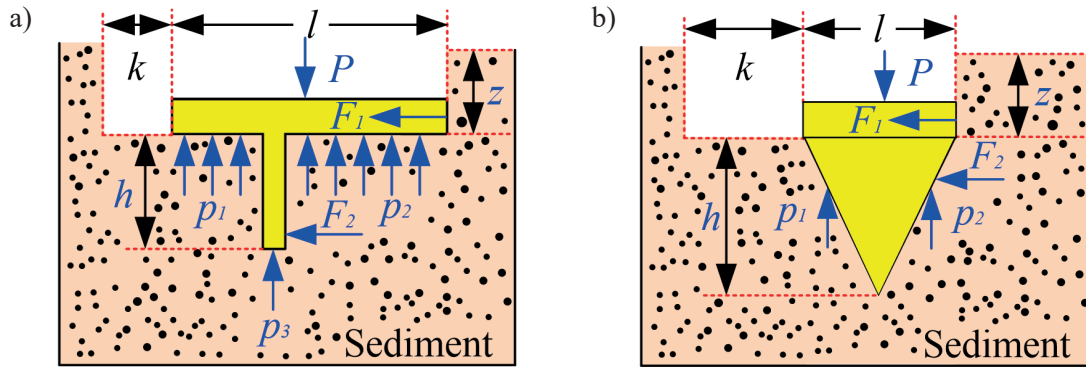


Fig. 6. The schematic diagram of track shoe shearing sediments

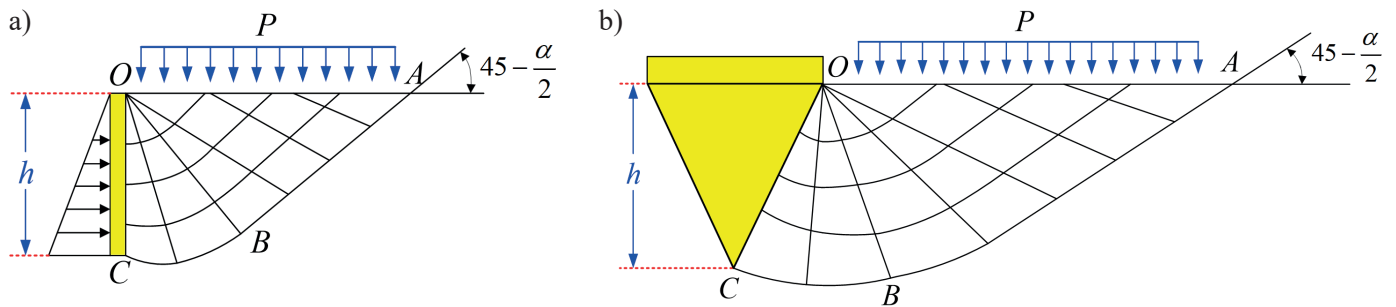


Fig. 7. The damage model of sediments in front of track shoe

shoe. p_1 , p_2 and p_3 are the interactive force implemented by the sediments, respectively.

The shear stress will be generated on the contact surface of the sediments and the track shoe when the sediments near the track shoe is in the plastic equilibrium state due to the friction and adhesion between the track shoe and the sediments. The damage models of sediments in front of the different tracks are shown in Fig. 7a and Fig. 7b. P is the total pressure implemented on the track. h is the track shoe height. α is the shear strength angle.

The tractive force can be obtained by the integral of the shear stress on the ground. The diagram of shear displacement

distribution of tracks that sink in the sediments is shown in Fig. 8.

The tractive force model proposed by Wang is employed in this study [44], which is shown as following,

$$\begin{aligned}
 F_T = & k_{pm} \left\{ \frac{k_w}{2i \cdot (2n_t L_t)} \left[e^{\frac{-i \cdot (2n_t L_t)}{k_w}} - 2c_{pm} \right]^2 + \right. \\
 & \left. + (2c_{pm} - 1) \left[1 + (2c_{pm} - 1) \cdot \frac{k_w}{2i \cdot (2n_t L_t)} \right] \right\} \cdot \\
 & \cdot (B_s + 2h)(2n_t L_t) \tau_{\max} + \\
 = & k_{pr} \left\{ -\frac{k_w}{2i \cdot (2n_t L_t)} \left[e^{\frac{-i \cdot (2n_t L_t)}{k_w}} - 2c_{pr} \right]^2 + \right. \\
 & \left. + (2c_{pr} - 1) \left[1 + (2c_{pr} - 1) \cdot \frac{k_w}{2i \cdot (2n_t L_t)} \right] \right\} \cdot \\
 & \cdot (B_s + 2h)(2n_t L_t) \tau_{res},
 \end{aligned} \tag{8}$$

where, n_t is the track number in one side of UUTB, L_t is the track length, i is the slip ratio, B_s is the track width, h is the track shoe height.

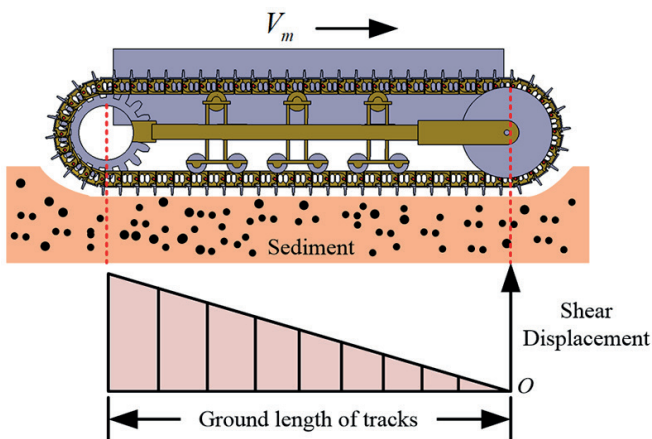


Fig. 8. The diagram of shear displacement distribution

It can be seen from Eq. (8) that most of the variables are coefficient, and the tractive force is mainly determined by track length, track width, track shoe height and the slip ratio. In this paper, the track length, track width and track shoe height of track 1, track 2 and track 3 are obtained from 3 different real tracks. Quantitative analysis is studied in this research. According to the above-mentioned reasons, the tractive force is just the function of the slip ratio of track 1, track 2 and track 3 under sand content 0%, 10% and 20%.

4. Experimental verification and analysis

The experiment is carried out to test the properties of the pressure-sinkage and shear stress-shear displacement between the track and configured sediment.

4.1. Experimental setup. The design drawing of the test platform is shown in Fig. 9a. The schematic of the testing system is shown in Fig. 9b. The configured sediment is mixed by ben-

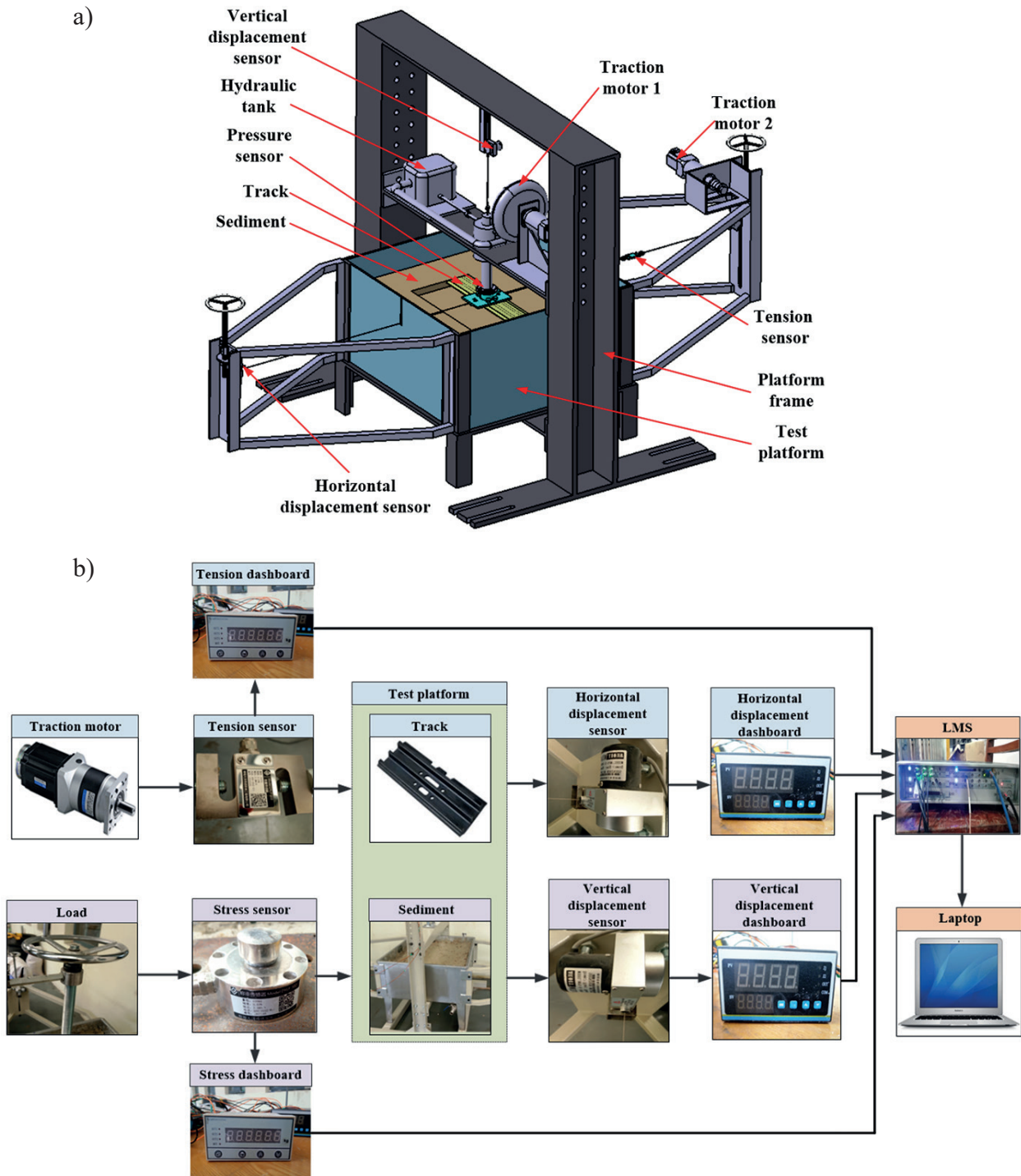


Fig. 9. The testing system: a) Test platform design drawing, b) The schematic of testing system

tonite, sand and water. The sand content in the sediment is configured as 0%, 10% and 20% to test the properties of the pressure-sinkage or shear stress-shear displacement between the track and sediment. The sediment should be soaked in the water to simulate the real sediment on the inland river bed. The sediment should be left at least 24 hours after each testing to ensure the pressure and shearing force distribute evenly.

4.2. Pressure-sinkage test under different sand content. The pressure-sinkage testing results of track 1, track 2 and track 3 under different sand content with dry basis moisture 115% are shown in Fig. 10. The pressure-sinkage testing results of different tracks under sand content 0%, 10% and 20% with dry basis moisture 115% are shown in Fig. 10. From Fig. 10a, the pressure-displacement test and fitting curves of track 1 under sand content 0%, 10% and 20% are marked with red, blue and black, respectively. It can be seen that the smaller the sand content, the larger sinkage of track 1 at 8 kPa. The pressure and sinkage test and fitting curves of track 2, shown in Fig. 10b, under sand content 0%, 10% and 20% are marked with red, blue and black, respectively. It also can be seen that the lower sand content, the larger sinkage of track 2 under the same pressure at 8 kPa. It can be obviously seen in Fig. 10c, the pressure and sinkage test and fitting curves of track 3 under sand content 0%, 10% and 20% are marked with red, blue and black, respectively. It also can

be seen that the smaller the sand content, the larger sinkage of track 3 under the same pressure at 8 kPa. The pressure-sinkage at 8 kPa with track 1, track 2 and track 3 under 0%, 10% and 20% are shown in Table 4.

Table 4
 Pressure-sinkage at 8 kPa with different sand contents of track 1, track 2 and track 3

Track	Track Sinkage (mm)		
	Sand content 0%	Sand content 10%	Sand content 20%
Track 1	71	53	36
Track 2	57	41	32
Track 3	125	83	57

To clearly show the relationship between pressure and sinkage, pressure-sinkage curves with different tracks under sand content 0%, 10% and 20% are shown in Fig. 11. From Fig. 11a, the pressure and displacement test and fitting curves of track 1, track 2 and track 3 under sand content 0% are marked with red, blue and black, respectively. From Fig. 11a, the pressure and displacement test and fitting curves of track 1 under sand content 0%, 10% and 20% are marked with red, blue and black,

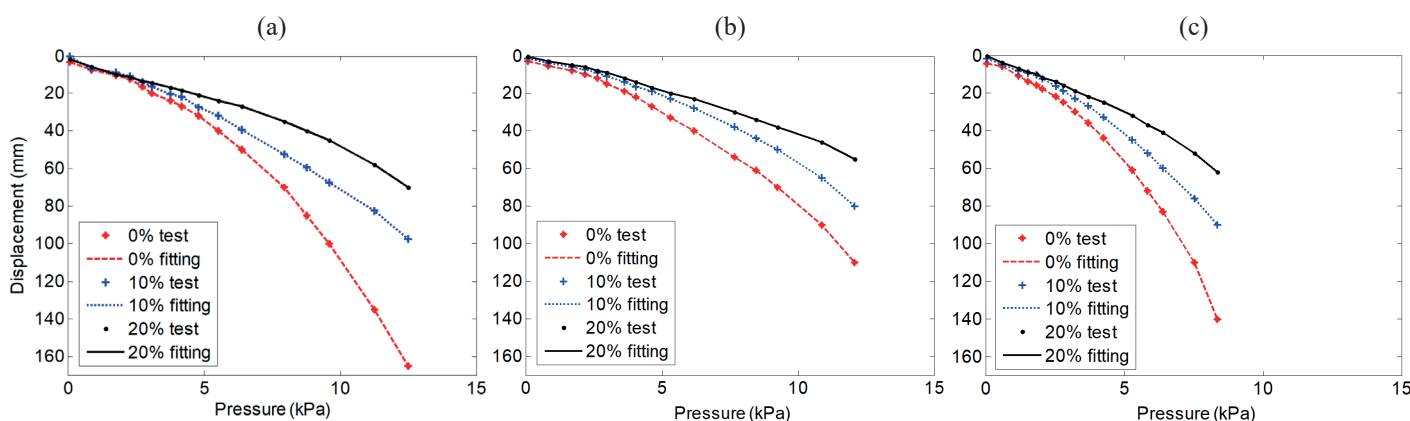


Fig. 10. Pressure-sinkage testing results under different sand content: a) Track 1, b) Track 2, c) Track 3

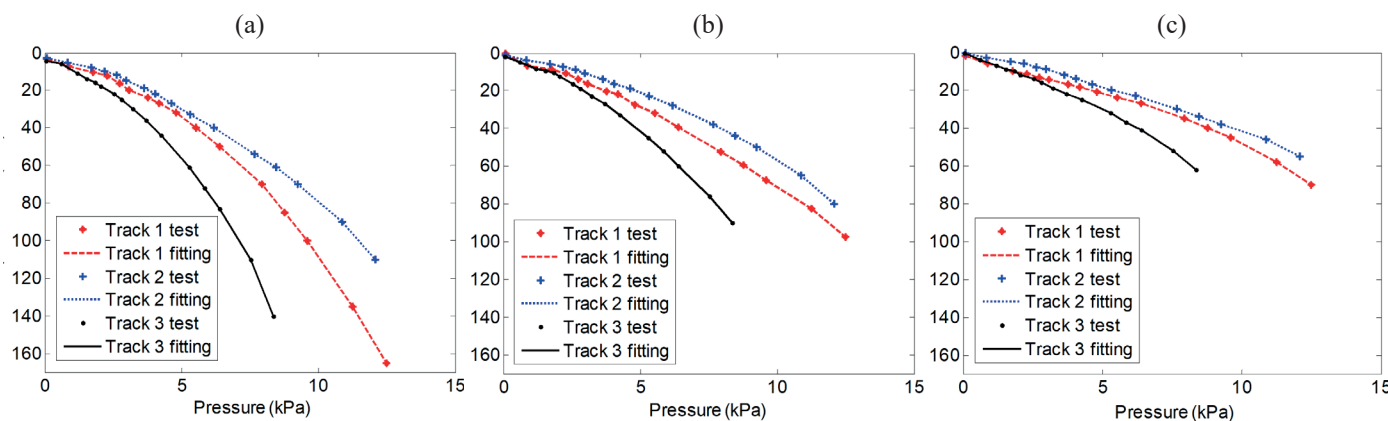


Fig. 11. Pressure-sinkage testing results with different tracks: a) Sand content 0%, b) Sand content 10%, c) Sand content 20%

respectively. From Fig. 11a, the pressure and displacement test and fitting curves of track 1 under sand content 0%, 10% and 20% are marked with red, blue and black, respectively. According to Bekker's model shown in Eq. (6), the modulus of cohesive deformation and friction deformation of the sediment with sand content 0%, 10% and 20% can be calculated, which are shown in Table 5.

Table 5
 Parameters of pressure sinkage with different sand content

Sand content	k_c	k_ϕ	n
0%	3.23	29.6	0.7
10%	7.98	26	0.73
20%	12.16	22	0.75

4.3. Shear stress-shear displacement test under different sand content. A constant load of 30 kg was implemented as normal pressure on the track during the shear stress-shear displacement testing. The shear stress and shear displacement test and fitting curves of track 1, track 2 and track 3 under sand content 0%, 10% and 20% with dry basis moisture 115% are shown in Fig. 12a, Fig. 12b and Fig. 12c, respectively. It can be seen from Fig. 12a, Fig. 12b and Fig. 12c, that the shear-

ing force increases rapidly at the beginning of the test and then achieves the summit value. After that, the shear stress decreases to a constant value. The Wang's shear stress-shear displacement model is employed to fit with the test data. It can be seen the test and fitting curves shown in Fig. 12 agree with the curve in Fig. 2. The shear stress increases sharply with the shear displacement in the beginning. After that, the shear stress drops sharply after its peak value. Then, the shear stress slowly reduces to a stable residual shear stress. However, the maximum values of the shear stress and the residual stress are totally different with different tracks under sand content 0%, 10% and 20%.

To present the relationship between the shear stress and shear displacement, the curves of test and fitting results of track 1, track 2 and track 3 under sand content 0%, 10% and 20% are shown in Fig. 13, Fig. 14 and Fig. 15. From top to bottom in Fig. 13 we can see the values of maximum shear stress, residual shear stress and maximum shear displacement of track 1 under sand content 0%, 10% and 20%, respectively. According to Wang's model in Eq. (5), the maximum shear stress, the residual shear stress and the shear displacement at the maximum shear stress can be obtained by the test results in Fig. 13. The shear strength-strength displacement testing results of track 2, under sand content 0%, 10% and 20% are shown in Fig. 14. According to Wang's model, the maximum

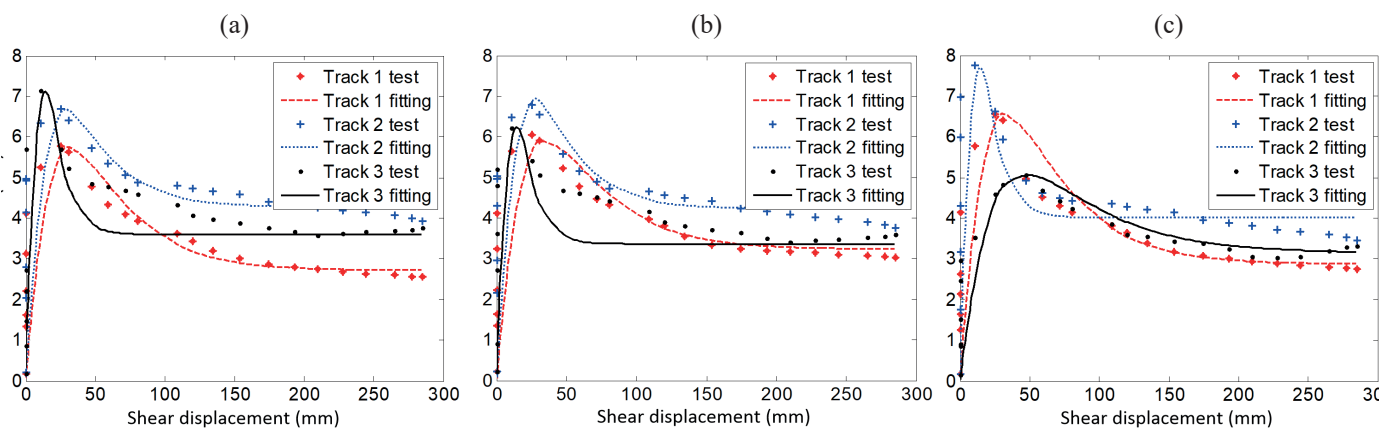


Fig. 12. Shear stress-shear displacement testing results under different sand content: a) Sand content 0%, b) Sand content 10%, c) Sand content 20%

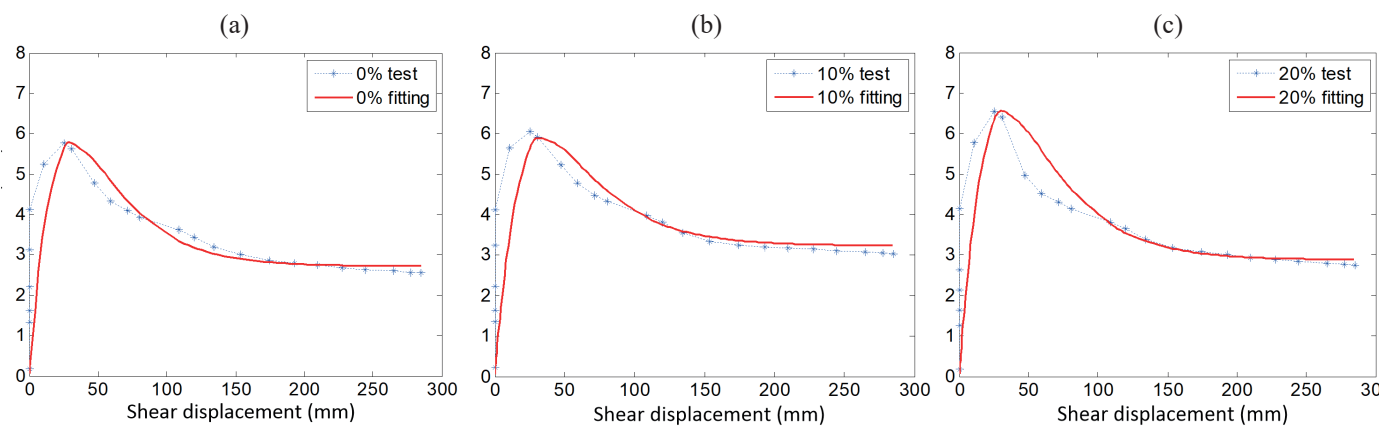


Fig. 13. Shear stress-shear displacement testing results with track 1: a) Sand content 0%, b) Sand content 10%, c) Sand content 20%

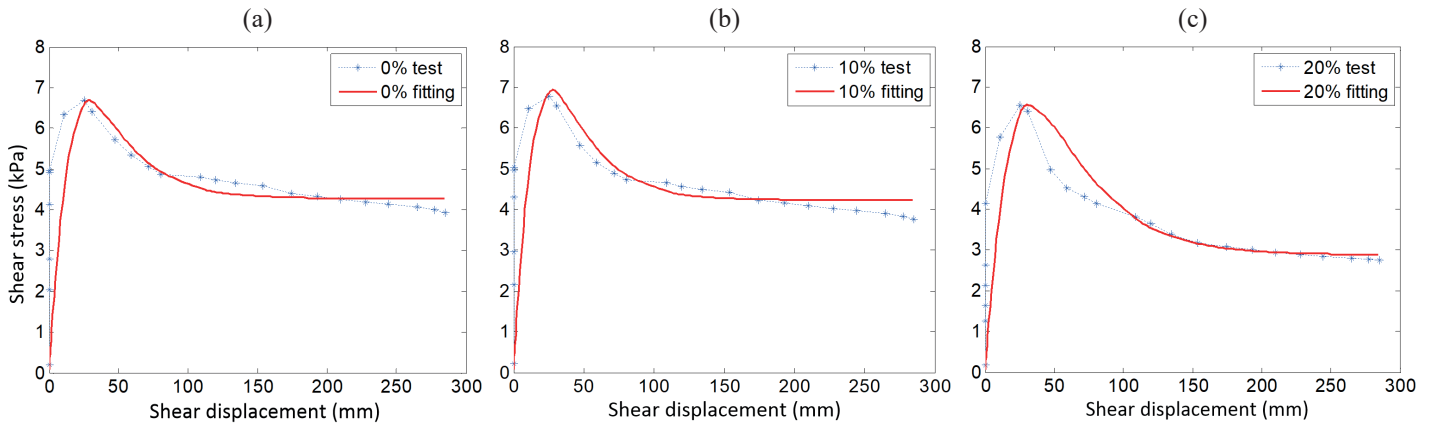


Fig. 14. Shear stress-shear displacement testing results with track 2: a) Sand content 0%, b) Sand content 10%, c) Sand content 20%

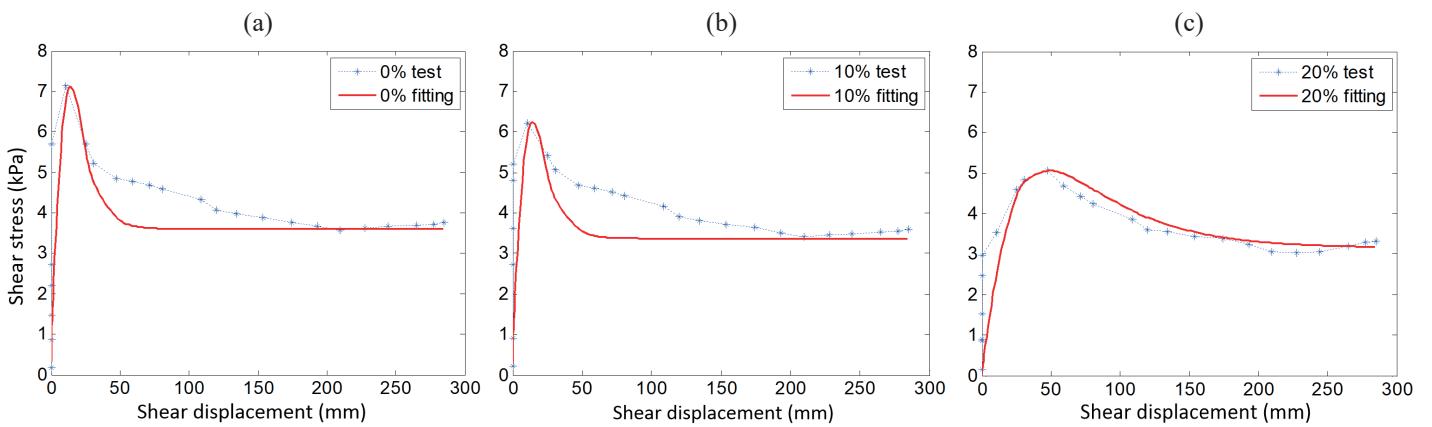


Fig. 15. Shear stress-shear displacement testing results with track 3: a) Sand content 0%, b) Sand content 10%, c) Sand content 20%

shear stress, the residual shear stress and the shear displacement at the maximum shear stress can be obtained by the test results in Fig. 14. The shear strength-shear displacement testing results of track 3, under sand content 0%, 10% and 20% are shown in Fig. 15. According to Wang’s model, the maximum shear stress, the residual shear stress and the shear displacement at the maximum shear stress can be obtained by the test results in Fig. 15.

From Fig. 13, Fig. 14 and Fig. 15, parameters can be seen, such as the correction factor caused by the soft-plastic deformation loss in hump zone, the correction factor caused by the soft-plastic deformation loss in residual zone, the adjustment conflict of the hump part and the adjustment coefficient of the residual part with different tracks under sand content 0%, 10%

and 20% can be obtained using Wang’s fitting model. The values of the above-mentioned model parameters of three tracks under sand content 0%, 10% and 20% are shown in Tables 6–8, respectively.

Table 7
 Model parameters of shear stress-shear displacement with sand content 10%

Sand content	Track	c_{pm}	c_{pr}	k_{pm}	k_{pr}
10%	Track 1	0.56	0.63	3.6	1.1
	Track 2	0.65	0.76	4.4	1.8
	Track 3	0.63	0.71	4.1	1.6

Table 6
 Model parameters of shear stress-shear displacement with sand content 0%

Sand content	Track	c_{pm}	c_{pr}	k_{pm}	k_{pr}
0%	Track 1	0.54	0.68	3.8	0.8
	Track 2	0.61	0.72	4.9	1.5
	Track 3	0.59	0.76	4.3	1.2

Table 8
 Model parameters of shear stress-shear displacement with sand content 20%

Sand content	Track	c_{pm}	c_{pr}	k_{pm}	k_{pr}
20%	Track 1	0.51	0.72	4.1	1.6
	Track 2	0.66	0.79	4.2	1.8
	Track 3	0.51	0.67	4.6	1.2

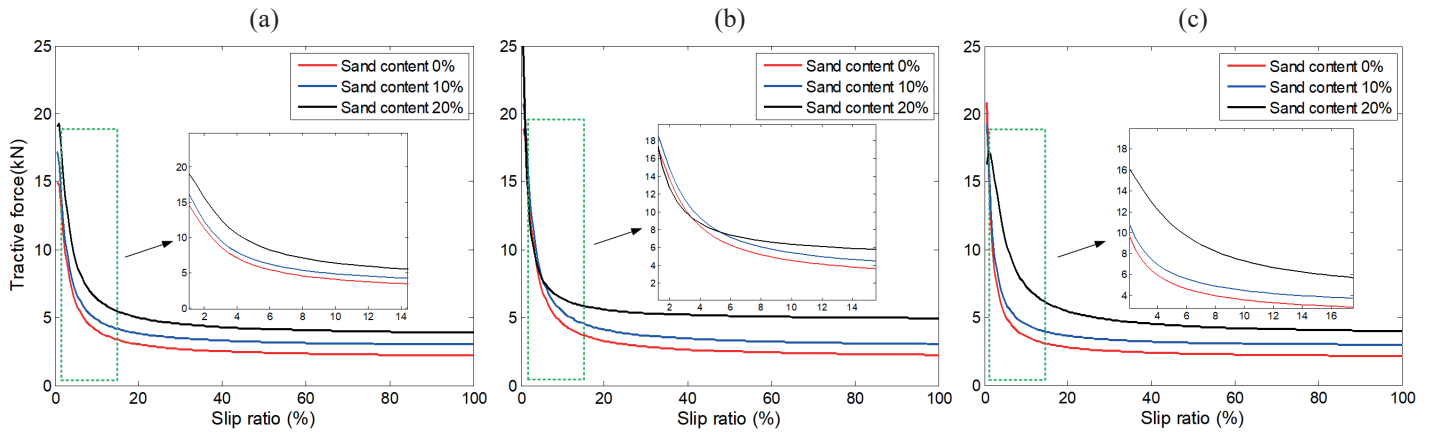


Fig. 16. Curves of tractive force vs. slip ratio under sand content 0%, 10% and 20%: a) Track 1, b) Track 2, c) Track 3

4.4. Tractive force performance discussion. The tractive force used to propel the UUTB is produced by the shearing force while it is operating on the sediments of the inland river. The relationship between the tractive force and slip ratio with sand content 0%, 10% and 20% are shown in Fig. 16. It can be seen from Fig. 16a, Fig. 16b and Fig. 16c that the tractive force decreases sharply with the increase of the slip ratio from 2% to 15%, then keeps at a constant value. From Fig. 16a it can be seen that the higher the sand content, the higher the tractive force of track 1 under the same slip ratio. The tractive force drops to a small value when the slip ratio is more than 20%. From Fig. 16b we can see the tractive force of track 2 changes with the sand content from 0% to 20%. The tractive force under sand content 20% is lower than that under 0% and 10%. However, it becomes higher when the slip ratio increases from 6%. The tractive force drops to a small value when the slip ratio is more than 20%. Figure 16c shows that the higher the sand content, the higher the tractive force of track 3 under the same slip ratio. The tractive force also drops to a small value when the slip ratio is more than 20%.

It can be concluded from Fig. 16a, Fig. 16b and Fig. 16c that the sand content has a certain influence on the shearing stress of the sediments, which provides different tractive force. The largest tractive force is generated when the slip ratio is larger than 1% and less than 6% for track 1, track 2 and track 3. The higher the sand content at the same slip ratio, the more tractive force will be generated for different tracks. It is suggested that the slip ratio should be controlled less than 6% to avoid the reduction of tractive force and propel the UUTB on the soft sediments of the inland river bed.

5. Conclusions

This paper focuses on the pressure-sinkage and shear stress-shear displacement between track and sediment. The conclusions are summarized as follows. The sediments with sand content 0%, 10% and 20% are configured to simulate the real sediments. The modulus of cohesive deformation and friction deformation of the sediment with sand content 0%,

10% and 20% are presented. The parameters such as maximum shear stress, residual shear stress, shear displacement at maximum shear stress, adjustment coefficient of hump part, adjustment coefficient of the residual part, correction factor caused by soft-plastic deformation loss in hump zone and correction factor caused by soft-plastic deformation loss in residual zone of different sediments under sand content 0%, 10% and 20% are obtained based on the experimental results of the properties between vertical pressure and sinkage with track 1, track 2 and track 3. The quantitative analysis of the relationship between the tractive force and slip ratio of three real tracks under sand content are investigated. The higher the sand content at the same slip ratio, the more tractive force will be generated for track 1, track 2 and track 3. The slip ratio should be controlled less than 6% to avoid the reduction of tractive force, which provides reference for the dynamics control and performance evaluation of the UUTB on the sediments of the inland river bed.

Future work will focus on the influence of track structure parameter on shear stress, tractive force, slip ratio and dynamic model of the UUTB.

Acknowledgements. This work was supported by the National Key R&D Program of China (2018YFC0810500).

REFERENCES

- [1] C.B. Yang, M. Dong, L. Gu, Q. Li, X.D. Gao, "Study on soil thrust of crawler plate considering the shape of shoe thorn", *J. Beijing Inst. Technol.* 35(11), 1118–1121 (2015).
- [2] C.B. Yang, *Research on the adhesion characteristics and optimization of high-speed track and soft ground*, Beijing Institute of Technology, 2015.
- [3] X. Lü, Q. Zhou, and B. Fang, "Hydrodynamic performance of distributed pump-jet propulsion system for underwater vehicle," *J. Hydrodyn.* 26(4), 523–530 (2014).
- [4] A. Yasui, K. Sunobe, and T. Murata "Development of underwater bulldozer systems", *J. Terramech.* 10(4), 13–20 (1973).
- [5] G. Yamauchi, K. Nagatani, T. Hashimoto, and K. Fujino "Slip-compensated odometry for tracked vehicle on loose and weak slope", *J. Hydrodyn.* 4(2), 2197–4225 (2017).

- [6] F. Xu, Q.H. Rao, and W.B. Ma, "Predicting the sinkage of a moving tracked mining vehicle using a new rheological formulation for soft deep-sea sediment", *J. Hydrodyn.* 36, 230–237 (2018).
- [7] S. Hong, J.S. Choi, H.W. Kim, M.C. Won, S.C. Shin, J.S. Rhee, and H.N. Par, "A path tracking control algorithm for underwater mining vehicles", *J. Mech. Sci. Technol.* 23(8), 2030–2037 (2009).
- [8] S.M. Yoon, S. Hong, S.J. Park, J.S. Choi, H.W. Kim, and T.K. Yeu, "Track velocity control of crawler type underwater mining robot through shallow-water test", *J. Mech. Sci. Technol.* 26(10), 3291–3298 (2012).
- [9] K. Herzog, E. Schulte, M.A. Atmanand, and W. Schwarz, "Slip Control System for a Deep-Sea Mining Machine", *IEEE Trans. Autom. Sci. Eng.* 4(2), 282–286 (2007).
- [10] H. Grebe and E.S. Schulte, *Determination of soil parameters based on the operational data of a ground operated tracked vehicle*, pp. 149–156, International Society of Offshore and Polar Engineers, 2005.
- [11] E. Schulte and W. Schwarz, "Simulation of Tracked Vehicle Performance on Deep Sea Soil Based on Soil Mechanical Laboratory Measurements in Bentonite Soil", in *Proceedings of The Eighth ISOPE Ocean Mining Symposium*, 2009, pp. 276–284.
- [12] L.Q. Song, "Geotechnical Properties of Oceanic Sediments in Polymetallic Nodules Belts", *Acta Oceanol. Sin.*, 19(2), 57–67 (2000).
- [13] X.L. Chen, J.Z. Lu, T.W. Cui, L.Q. Tian, L.Q. Chen, and W.J. Zhao, "Coupling remote sensing retrieval with numerical simulation for SPM study—Taking Bohai Sea in China as a case", *Int. J. Appl. Earth Obs. Geoinf.* 12(2), 203–211 (2010).
- [14] S.J. Liu, C. Liu, and Y. Dai, "Research and development of deep-sea mining equipment", *Chin. J. Mech. Eng.* 50(2), 8–18 (2014).
- [15] Y. Dai and S.J. Liu, "Dynamic analysis of integrated linkage operation mode of deep-sea mining system", *J. Huazhong Univ. Sci. Tech.-Natural Sci.* 40(S2), 39–43 (2012).
- [16] Y. Dai and S.J. Liu, "Theoretical design and dynamic simulation of new mining paths of tracked miner on deep seafloor", *J. Cent. South Univ.* 20(04), 918–923 (2013).
- [17] Y. Dai and S.J. Liu, "Dynamic Analysis of the Seafloor Pilot Miner Based on Single-Body Vehicle Model and Discretized Track-Terrain Interaction Model", *China Ocean Eng.* 24(01), 145–160 (2010).
- [18] Y. Dai, H. Liu, T. Zhang, and S.J. Liu, "A study on the driving performance of seabed crawler mining vehicle", *Chinese Sci. Technol. Paper* 10(10), 1203–1208 (2015).
- [19] L. Li and S.L. Li, "Simulation of deep-sea surface Marine mud and study on surface mechanical properties", *Eng. Mech.* 27(11), 213–220 (2010).
- [20] M. Wang, X. Wang, and Y. Sun, "Tractive performance evaluation of seafloor tracked trencher based on laboratory mechanical measurements", *Int. J. Nav. Archit. Ocean Eng.* 8(2), 177–187 (2016).
- [21] M. Wang, X. Wang, and Y. Sun, "Traction Potential Analysis of Self-Propelled Seafloor Trencher Based on Mechanical Measurements in Bentonite Soil", *J. Harbin Inst. Technol.* 24(1), 71–80 (2017).
- [22] C. Yang, G. Yang, and Z. Liu, "A method for deducing pressure–sinkage of tracked vehicle in rough terrain considering moisture and sinkage speed", *J. Terramech.* 79, 99–113 (2018).
- [23] P. Siemaszko and Z. Meyer, "Static load test cure analysis based on soil field investigations", *Bull. Pol. Ac.: Tech.* 67(2), 329–337 (2019).
- [24] A. Sawicki, J. Mierczynski, and W. Swidzinski, "Basic set of experiments for determination of mechanical properties of sand", *Bull. Pol. Ac.: Tech.* 62(1), 129–137 (2014).
- [25] C. Janarthanan, K. Gopkumar, V. Sundaramoorthi, N.R. Ramesh, and G.A. Ramadass, "Influence of Grouser Geometrical Parameters of Deep-Sea Crawler Vehicle on Soft Clays", *J. Hydrodyn.* 47:899–912 (2018).
- [26] H. Mao, F. Kumi, and Q. Li, "Combining X-ray computed tomography with relevant techniques for analysing soil-root dynamics—an overview", *Acta Agric. Scand. Sect. B – Soil Plant Sci.* 66(1), 1–19 (2015).
- [27] T. Kato and M. Kamichika, "Determination of a crop coefficient for evapotranspiration in a sparse sorghum field", *Irrig. Drain.*, 55(2), 165–175 (2010).
- [28] S. Hong, H.W. Kim, T. Yue, J.S. Choi, T.H. Lee, and J.K. Lee, "Technologies for Safe and Sustainable Mining of Deep-Seabed Minerals", *J. Hydrodyn.* 65:95–143 (2019).
- [29] Z.Y. Zuo, X.G. Li, C. Xu, "Responses of barley Albina and Xantha mutants deficient in magnesium chelatase to soil salinity", *Plant Soil Environ.* 63(8), 348–354 (2017).
- [30] C.L. Qi, Q.H. Rao, Q. Liu, and W.B. Ma, "Traction rheological properties of simulative soil for deep-sea sediment", *J. Hydrodyn.* 37:61–71 (2019).
- [31] B. Ali Abubaker, H.F. Yan, and L. Hong, "Enhancement of Depleted Loam Soil as Well as Cucumber Productivity Utilizing Biochar Under Water Stress", *Commun. Soil Sci. Plant Anal.* 50(1), 49–64 (2019).
- [32] W. Wei, Y. Xu, and S. Li, "Developing suppressive soil for root diseases of soybean with continuous long-term cropping of soybean in black soil of Northeast China", *Acta Agric. Scand. Sect. B – Soil Plant Sci.* 65(3), 7 (2015).
- [33] J.Z. Li, S.J. Liu, and Y. Dai, "Effect of grouser height on tractive performance of tracked mining vehicle", *J. Hydrodyn.* 39:2459–2466 (2017).
- [34] D. Knez and A. Calicki, "Looking for a new source of natural proppants in Poland", *Bull. Pol. Ac.: Tech.* 66(1), 3–8 (2018).
- [35] M. Mitew-Czajewska, "Parametric study of deep excavation in clays", *Bull. Pol. Ac.: Tech.* 66(5), 747–754 (2018).
- [36] J. Liu, X.M. Liu, and J.M. Xie, "Influence of copper on transport and dissipation of lambda-cyhalothrin and cypermethrin in soils", *Pedosphere* 23(3), 395–401 (2013).
- [37] L.L. Chu, Y.H. Kang, and S.Q. Wan, "Effect of different water application intensity and irrigation amount treatments of microirrigation on soil-leaching coastal saline soils of North China", *J. Integr. Agric.* 15(9), 2123–2131 (2016).
- [38] J.Y. Wong, *Theory of Ground Vehicles*. John Wiley & Sons Inc, 2001.
- [39] J.Y. Wong, *Terramechanics and Off-road Engineering*. Elsevier, 2010.
- [40] J.Y. Wong, M. Garber, and J. Preston-Thomas, "Theoretical prediction and experimental substantiation of the ground pressure distribution and tractive performance of tracked vehicles", *Proc. Inst. Mech. Eng. Part D-J. Automob. Eng.* (4), 265–285 (1988).
- [41] E. Schulte, R. Handschuh, and W. Schwarz, "Transferability of soil mechanical parameters to traction potential calculation of a tracked vehicle", in *Proceedings of the Fifth Ocean Mining Symposium*, 2003, pp. 123–131.
- [42] Z. Janosi and B. Hanamoto, "Analytical determination of drawbar pull as a function of slip on tracked vehicles in deformable soils", *1st Intern. Conference on Terrain-Vehicles Systems*, 1961, pp. 1131–1152.

- [43] M. Wang, C. Wu, and T. Ge, “Calibration and validation of tractive performance for seafloor tracked trencher”, *J. Terramech.* 66, 13–25 (2016).
- [44] M. Wang, X.Y. Wang, Y.H. Sun, and Z.M. Gu, “Tractive performance evaluation of seafloor tracked trencher based on laboratory mechanical measurements”, *Int. J. Nav. Archit. Ocean Eng.* 8, 177–187 (2016).
- [45] M.G. Bekker, *Theory of land locomotion: the mechanics of vehicle mobility*, pp. 221–262, The University of Michigan Press, 1956.
- [46] M.G. Bekker, *Theory of Land Locomotion*, University of Michigan Press, 1962.
- [47] M.G. Bekker, *Introduction to Terrain-vehicle Systems*, University of Michigan Press, 1969.
- [48] A.R. Reece, “Principles of soil-vehicle mechanics”, *Proc. Inst. Mech. Eng. Automob. Div.* 180(1), 45–66 (1965).
- [49] Y. Xu, H.Y. Wu, and L.B. Zuo, “Influence of shale tooth height of tracked vehicle on traction performance and its parameter determination”, *Trans. Chinese Soc. Agric. Eng.* 28(11), 68–74 (2012).